

Impact of ocean variability on coherent underwater acoustic communications during the Kauai experiment (KauaiEx)

Aijun Song^{a)} and Mohsen Badiey

College of Marine and Earth Studies, University of Delaware, 114 Robinson Hall, Newark, Delaware 19716

H. C. Song and William S. Hodgkiss

Marine Physical Laboratory, Scripps Institution of Oceanography, La Jolla, California 92093-0238

Michael B. Porter and the KauaiEx Group

Heat, Light, & Sound Research Inc., 3366 North Torrey Pines Court, Suite 310, La Jolla, California 92037

(Received 6 September 2007; revised 15 November 2007; accepted 24 November 2007)

During the July 2003 acoustic communications experiment conducted in 100 m deep water off the western side of Kauai, Hawaii, a 10 s binary phase shift keying signal with a symbol rate of 4 kilosymbol/s was transmitted every 30 min for 27 h from a bottom moored source at 12 kHz center frequency to a 16 element vertical array spanning the water column at about 3 km range. The communications signals are demodulated by time reversal multichannel combining followed by a single channel decision feedback equalizer using two subsets of array elements whose channel characteristics appear distinct: (1) top 10 and (2) bottom 4 elements. Due to rapid channel variations, continuous channel updates along with Doppler tracking are required prior to time reversal combining. This is especially true for the top 10 elements where the received acoustic field involves significant interaction with the dynamic ocean surface. The resulting communications performance in terms of output signal-to-noise ratio exhibits significant change over the 27 h transmission duration. This is particularly evident as the water column changes from well-mixed to a downward refracting environment. © 2008 Acoustical Society of America. [DOI: 10.1121/1.2828055]

PACS number(s): 43.60.Dh, 43.60.Gk, 43.60.Fg, 43.60.Mn [EJS]

Pages: 856–865

I. INTRODUCTION

Underwater acoustic channels are challenging for coherent digital communications because of severe multipath spread and limited bandwidth. Further, the variability of the ocean environment can cause fast fluctuations of acoustic channels and these fluctuations result in additional limitations on digital communications. Since the 1990s, various investigations on decision feedback equalizers (DFEs) and time reversal approaches have contributed to the advancement of coherent underwater acoustic communications. It has been shown that the DFE coupled with a phase tracking process presents a practical solution to the multi-path spread and fast phase fluctuation of underwater acoustic channels.¹ The DFE with joint phase tracking can be extended to multiple hydrophone channels to form a multichannel DFE.² In the multichannel DFE, the total number of adaptive feedforward taps increases with the number of channels. The implementation complexity of the multichannel DFE is high for a moderate to large number of hydrophone channels, which often are needed to achieve reliable performance in dynamic ocean environments. In order to alleviate the complexity issue, channel estimation can be incorporated into the DFE structure.³

Time reversal processing is able to achieve pulse compression for transmissions that have been spread by propagation through a multipath ocean environment. The time rever-

sal concept was first demonstrated in the ocean in the 1960s.^{4,5} Since the late 1990s, applications of the physics-based time reversal principle in underwater acoustic communications have shown success in at-sea experiments. Both active^{6–8} and passive^{9–11} time reversal methods have been investigated where in the latter, only one-way transmissions are used at a receiving array to implement the time reversal process. More recently, the time reversal approach has been combined with DFEs to improve the receiver performance while providing low implementation complexity.^{12–15} In these studies, the acoustic channels usually are assumed time-invariant or slowly varying.

Over the last several years, a few studies have shown that correlation exists between high frequency acoustic fluctuations and environmental characteristics.^{16–18} For example, the effects of tidally driven temperature fluctuations on underwater coherent acoustic communications have been studied at a carrier frequency of 18 kHz.¹⁶ However, the relationship between environmental fluctuations and the performance of coherent underwater acoustic communications is not fully understood yet.

The Kauai experiment (KauaiEx) was conducted in June and July of 2003 to study high frequency (8–50 kHz) acoustic communications in 100 m deep water near Kauai, Hawaii.^{19,20} During KauaiEx, extensive acoustic measurements were conducted while the ocean environment was monitored. The binary phase shift keying (BPSK) signals which were transmitted over an extended period (27 h) during KauaiEx are discussed in this paper. The communications signals are demodulated by time reversal multichannel

^{a)}Electronic mail: ajsong@udel.edu.

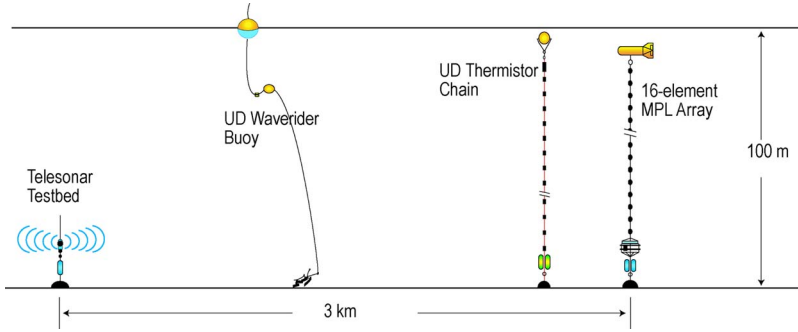


FIG. 1. (Color online) KauaiEx was conducted west of Kauai, HI, in 100 m deep water. The bottom-mounted Telesonar Testbed acoustic source was deployed 5 m above the sea bottom. At about 3 km range, the 16 element MPL autonomous receiving array spanned the entire water column. The wave-rider buoy was deployed about 1.2 km from the source. The thermistor chain shown was about 400 m from the MPL array.

combining followed by a single channel DFE. Acoustic channels in KauaiEx exhibited fast variations at a center frequency of 12 kHz in dynamic ocean environments. Therefore, continuous channel updates along with Doppler tracking are required prior to time reversal combining in order to track channel fluctuations. The performance of the communications receiver in terms of output signal-to-noise ratio (SNR) is reported over the entire 27 h transmission duration.

This paper is organized as follows. In Sec. II, a brief introduction to KauaiEx is presented. The receiver structure is presented in Sec. III. The acoustic channel and the BPSK performance are shown in Sec. IV. In the paper, a variable

with superscript (i) denotes the value at the i th hydrophone. A variable with a caret denotes the estimate of the variable. c^* denotes the complex conjugate of a complex number c . $a(n)*b(n)$ denotes the convolution of two sequences $a(n)$ and $b(n)$. All time information regarding the experiment is in Greenwich Mean Time (GMT) if not otherwise stated.

II. KAUAIEX

KauaiEx was conducted from June 22 to July 9, 2003, west of Kauai, HI, in a shallow water waveguide.¹⁹ The experiment data during July 2 through July 3, 2003, are of

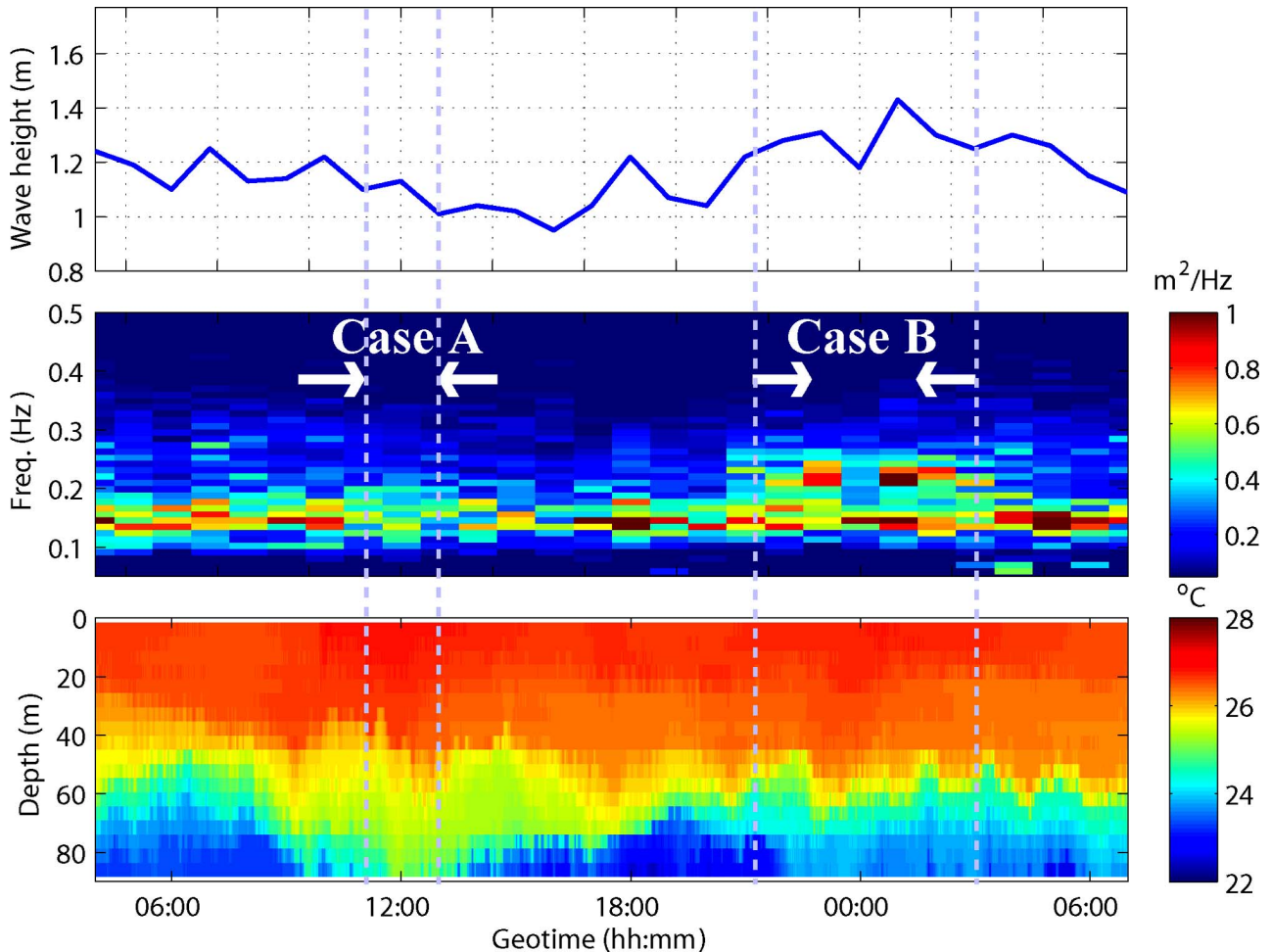


FIG. 2. (Color online) Environmental characteristics. Top panel: Significant wave height; Middle panel: Surface wave spectrum; Bottom panel: Temperature profile from 04:00 on July 2 to 07:00 on July 3, 2003, in KauaiEx. Note around 12:00 on July 2 (Case A), the water column was well mixed and the sea surface was relatively calm. From 21:00 on July 2 to 03:00 on July 3 (Case B), the water column was stratified and the sea surface was rougher.

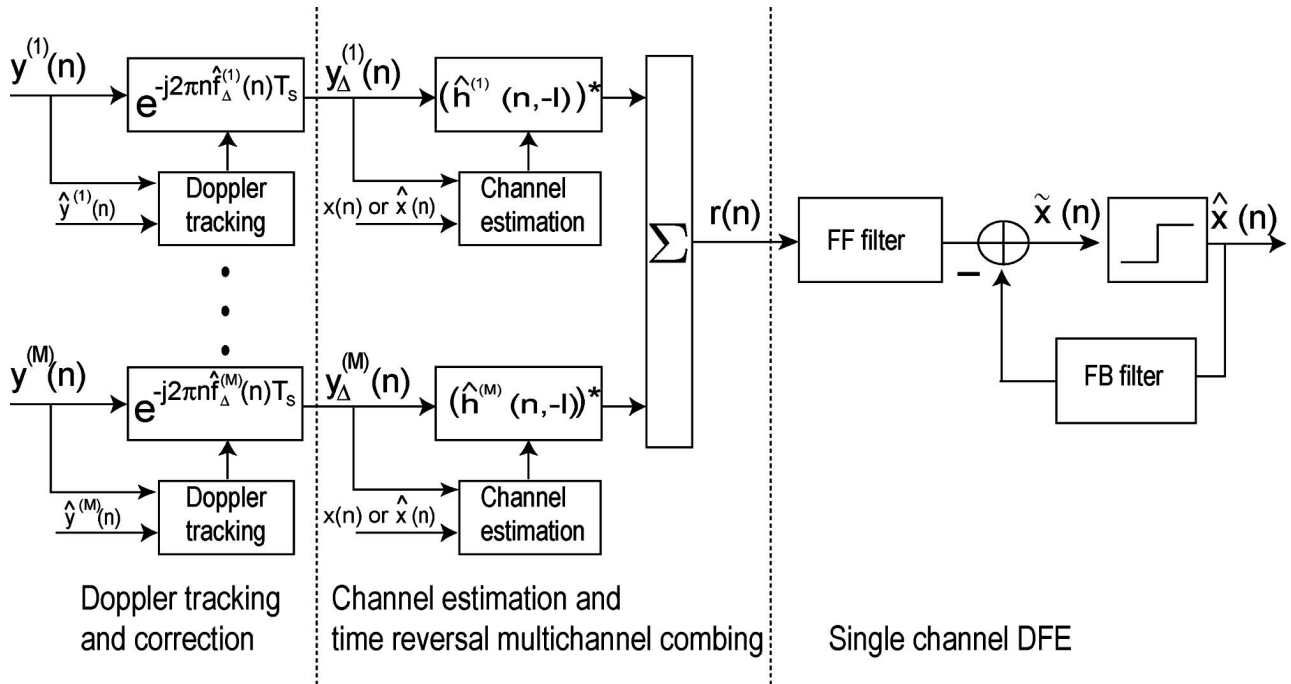


FIG. 3. The proposed receiver is composed of three parts: (1) Doppler tracking and correction, (2) channel estimation and time reversal multichannel combining, and (3) single channel DFE.

interest in this paper. As shown in Fig. 1, the water depth of the experimental site was 100 m. The Telesonar Testbed²¹ was deployed 5 m above the sea bottom and served as the acoustic source. The source power level was 183 dB re 1 μ Pa at 1 m. At about 3 km range, a 16 element Marine Physical Laboratory (MPL) autonomous receiving array spanned the entire water column. The spacing of the hydrophones was 5 m. The top hydrophone was 16.5 m below the sea surface. Of a series of high frequency acoustic signals transmitted by the Telesonar Testbed, the 10 s BPSK signal will be used in the analysis. The carrier frequency of the BPSK signal is $f_c=12$ kHz and the symbol rate is $R=4$ kilosymbols/s. The square-root raised cosine shaping filter is used with an excess bandwidth²² of 100%. The 10 s BPSK signal is referred to as a BPSK packet. The BPSK packet was transmitted and received every 30 min for 27 h from 04:00 on July 2 to 07:00 on July 3, 2003. In addition, 8–14 kHz, 50 ms long linear frequency modulated (LFM) chirps were transmitted a minute prior to every BPSK packet. The received waveforms on the MPL array were sampled at $f_s=50$ kHz.

Along with acoustic measurements, the surface wave spectrum and the two-dimensional water temperature profile were measured by a wave-rider buoy and a series of thermistor chains deployed along the propagation path. The wind speed underwent a late morning (Hawaii local time 10:00 a.m., e.g., 20:00 GMT) increase and a late night decrease as indicated by the sea surface wave spectrum in the middle panel of Fig. 2. The corresponding significant wave height varied from 1.4 to 1.0 m as shown in the top panel of Fig. 2. The water temperature profile shown in the bottom panel of Fig. 2 was measured by a thermistor chain deployed about 400 m from the MPL array. Note that for most of the time the water column was well mixed down to about 50 m depth.

A cold layer (about 4–5 °C lower than the mixed layer) emerged at nearly tidal cycles. In addition to the communication results for the entire 27 h period, acoustic data during two contrasting environmental conditions marked as Case A and Case B in Fig. 2 will be discussed. Case A corresponds to around 12:00 on July 2 when the sea surface was relatively calm and the water column was well mixed. Case B is from 21:00 on July 2 to 03:00 on July 3 when the sea surface was slightly rougher and the water column was stratified. The main contrast between Cases A and B is the stratification of the water column. The significant wave height during Case A was about 1.1 m versus about 1.3 m during Case B.

III. THE RECEIVER STRUCTURE

Consider an underwater acoustic transmitter and receiver deployed in shallow water. At the source, a binary information sequence $x(n)$ is transformed into the baseband continuous wave $x(t)$. Then $x(t)$ is modulated onto the carrier frequency f_c and transmitted from a sound transducer. The receiver usually is equipped with multiple hydrophones. Let the total number of the hydrophones be M and $y^{(i)}(t)$ be the received baseband signal at the i th hydrophone. The effect of the transmission medium between the source and the i th hydrophone can be characterized by a time-varying channel impulse response (CIR) function, $h^{(i)}(t, \tau)$. The analog waveform $y^{(i)}(t)$ is sampled at a fractional symbol interval to provide robustness to carrier phase fluctuations in the underwater acoustic channel.^{2,22} However, for notation convenience, symbol spaced signals are used throughout the paper. Therefore,

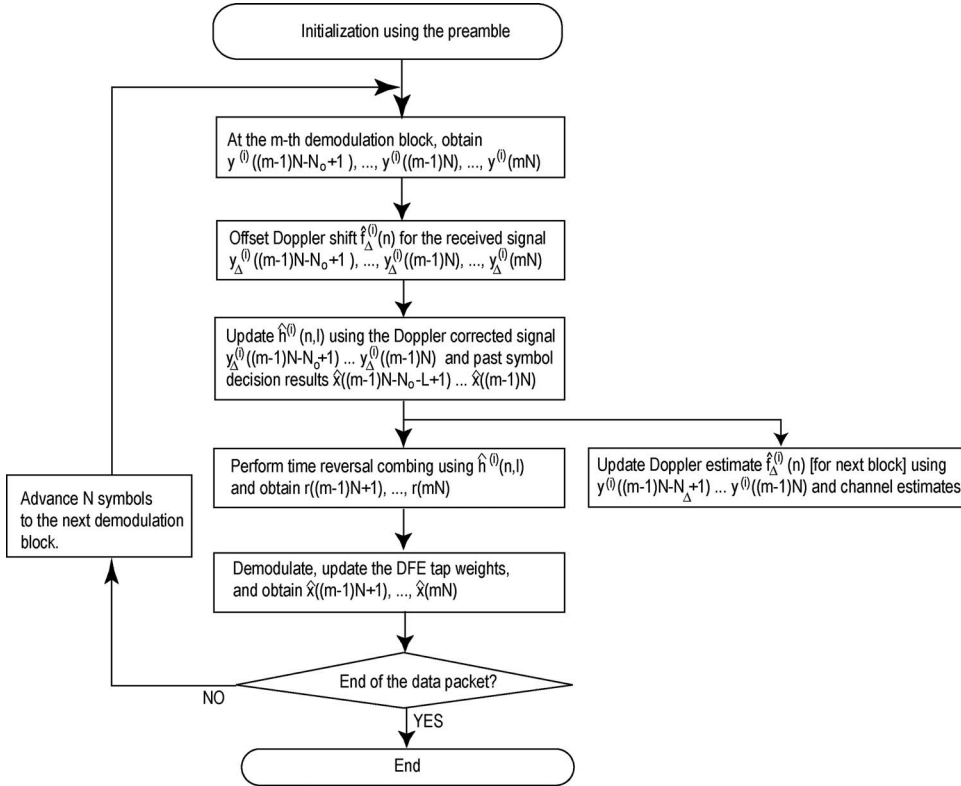


FIG. 4. The flow diagram of the receiver. Without loss of generality, $N_0 \geq N_\Delta$ is assumed.

$$y^{(i)}(n) = e^{j\theta^{(i)}(n)}[x(n) * h^{(i)}(n,l)] + v_{\text{amb}}^{(i)}(n), \quad (1)$$

where $y^{(i)}(n)$ is the discrete time representation of the analog signal $y^{(i)}(t)$, $\theta^{(i)}(n)$ is the instantaneous carrier phase offset, and $T_s = 1/R$ is the symbol duration. $v_{\text{amb}}^{(i)}(n)$ represents the ambient noise. $h^{(i)}(n,l)$, $0 \leq l \leq L-1$, is the discrete time baseband CIR function where L is the duration in symbols. $h^{(i)}(n,l)$ includes the combined effects of transmitter/receiver filters and the CIR function.

To recover the transmitted symbols which have been passed through the time-varying multi-path acoustic waveguide, a new multichannel receiver structure is proposed. Several features are incorporated into the receiver structure: (1) continuous Doppler tracking and correction is used to compensate for any observed linear trend in the carrier phase offset, (2) frequent channel estimation is used to track channel fluctuations,^{3,23,24} and (3) compensation for residual phase fluctuations and intersymbol interference after time reversal combining is done using a DFE.¹ As shown in Fig. 3, the receiver consists of three parts: Doppler tracking and correction, channel estimation and time reversal multichannel combining, and single channel DFE.

The proposed receiver is a channel estimation based structure. At the beginning of a data packet, a preamble, or a sequence of known symbols, is used to perform initial channel and Doppler estimation and to train adaptively the DFE tap weights. After the preamble, channel and Doppler estimation are frequently updated. The most recent channel estimate on the i th channel is denoted by $\hat{h}^{(i)}(n,l)$ and the most recent Doppler estimate is denoted by $\hat{f}_\Delta^{(i)}(n)$. The three major parts of the receiver now will be discussed, followed by the overall implementation procedure.

A. Doppler tracking and correction

The Doppler estimate at the i th channel is obtained by

$$\hat{f}_\Delta^{(i)}(n) = \arg \max_{f_0^{(i)} - (1/2)\delta f < f < f_0^{(i)} + (1/2)\delta f} \left| \sum_{p=0}^{N_\Delta-1} y^{(i)}(n-p)(\hat{y}^{(i)}(n-p)e^{j2\pi p f T_s})^* \right|, \quad (2)$$

where $\hat{y}^{(i)}(n) = x(n) * \hat{h}^{(i)}(n,l)$ during the preamble and $\hat{y}^{(i)}(n) = \hat{x}(n) * \hat{h}^{(i)}(n,l)$ after the preamble. In Eq. (2), N_Δ is the Doppler observation block in symbols, $f_0^{(i)}$ is the coarse Doppler estimate and δf is the Doppler search range. Various Doppler estimation approaches exist in the literature, for example the ambiguity function method.²⁵

At the beginning of the BPSK packets, $f_0^{(i)}$ is assumed to be zero as no *a priori* information is available and the Doppler shift should be obtained by searching over a large range of values. After the initial synchronization, as Doppler is estimated frequently, $f_0^{(i)}$ is set to the previous Doppler estimate and δf can be small. The Doppler correction is performed by offsetting the received signal $y^{(i)}(n)$ by the estimated Doppler shift, i.e., $y_\Delta^{(i)}(n) = y^{(i)}(n)e^{-j2\pi n \hat{f}_\Delta^{(i)}(n) T_s}$.

B. Channel estimation and time reversal multichannel combining

The channel estimate $\hat{h}^{(i)}(n,l)$ can be obtained from the Doppler corrected received signal $y_\Delta^{(i)}(n)$ and the previously detected symbols $\hat{x}(n)$ or the known symbols $x(n)$ during the preamble. Various least squares algorithms can be used for channel estimation. In this paper, the iterative least squares

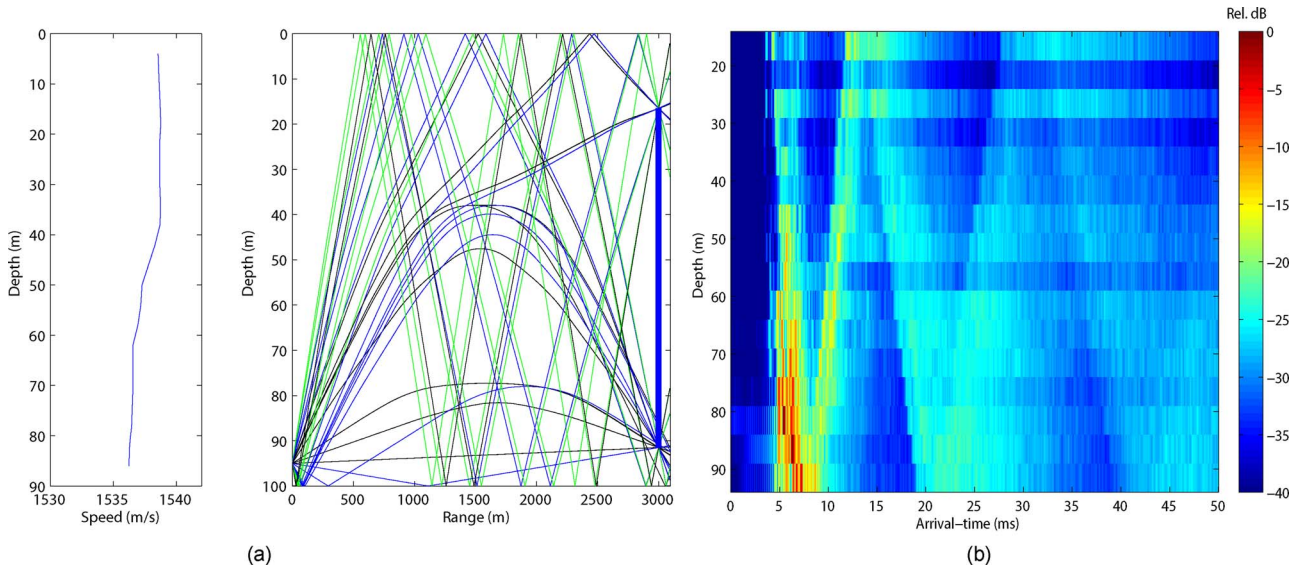


FIG. 5. (Color online) Acoustic propagation characteristics. (a) The sound speed profile (left-hand panel) and the ray diagram (right-hand panel) for the top and bottom hydrophones of the MPL array at 12:00 on July 2, 2003. (b) The CIR function obtained from the received LFM signals on the MPL array at 12:00 on July 2, 2003.

QR (LSQR) algorithm is used.²⁶ The channel estimation block size is chosen to be twice the channel length, i.e., $N_0 = 2L$.

Time reversal multichannel combining uses $(\hat{h}^{(i)}(n, -l))^*$ to match-filter the Doppler-corrected signals on each channel $y_{\Delta}^{(i)}(n)$ and then combines the results.^{6,7,9} The output of time reversal combining is

$$r(n) = \sum_{i=1}^M (\hat{h}^{(i)}(n, -l))^* * y_{\Delta}^{(i)}(n) = x(n) * q(n, l) + w(n), \quad (3)$$

where $w(n)$ is the noise component,

$$w(n) = \sum_{i=1}^M (\hat{h}^{(i)}(n, -l))^* * (v_{\text{amb}}^{(i)}(n) e^{-j2\pi n f_{\Delta}^{(i)}(n) T_s}), \quad (4)$$

and $q(n, l)$ is the effective CIR function, or the q -function,^{10,11,13}

$$q(n, l) = \sum_{i=1}^M (\hat{h}^{(i)}(n, -l))^* * h^{(i)}(n, l), \quad (5)$$

assuming the Doppler correction completely removes the instantaneous carrier phase offset $\theta^{(i)}(n)$.

C. The single channel DFE

A single channel DFE with joint phase tracking¹ is used to equalize the residual intersymbol interference in $r(n)$. The exponentially weighted recursive least-squares (RLS) algorithm is used to update the equalizer tap weights. The residual carrier phase offset in $r(n)$ is compensated for by a second order phase locked loop (PLL) embedded in the adaptive channel equalizer. The phase correction based on the PLL output is implemented at the input to the DFE feed-forward filter.

D. Implementation procedure

Figure 4 shows the implementation procedure for the proposed receiver. After the preamble at the beginning of each data packet, the receiver performs these tasks based on the previously detected symbols. Let the channel estimation update interval be N symbols with the receiver processing N symbols as a demodulation block each update. At the m th demodulation block, the receiver has obtained previously detected symbols through the $(m-1)$ th demodulation block, i.e., $\hat{x}(n)$, $n \leq (m-1)N$, is known, and the objective is to recover the current N symbols $x(n)$, $n = (m-1)N+1, \dots, mN-1, mN$. First, Doppler correction is made for the received signal at individual channels based on the most recent Doppler estimate $\hat{f}_{\Delta}^{(i)}(n)$. Subsequently, the channel estimate $\hat{h}^{(i)}(n, l)$ is updated using the Doppler corrected signals and the previously detected symbols. Note that Doppler tracking is performed again using the updated channel estimate for use in the next demodulation block. Then time reversal combining and equalization are conducted and the N symbol estimates $\hat{x}(n)$ are obtained. The algorithm advances to the next demodulation block if the end of the data packet has not been reached.

In the literature, existing DFE approaches include: (1) time reversal DFEs^{12–14} and (2) multichannel DFEs developed by Stojanovic *et al.*^{2,3} Although time reversal based, the proposed receiver has a different structure than the referenced time reversal DFEs where multichannel combining is performed based on channel probes or the known symbols at the beginning of the data packet. In the referenced time reversal DFEs,^{12–14} phase tracking or Doppler tracking usually is performed after time reversal combining. Then an adaptive DFE is used to compensate for residual sidelobe structure in the q -function [Eq. (5)] and phase fluctuations. Compared with the referenced time reversal DFEs, the proposed receiver performs continuous Doppler tracking and channel estimation to combat fast fluctuations which occur over the

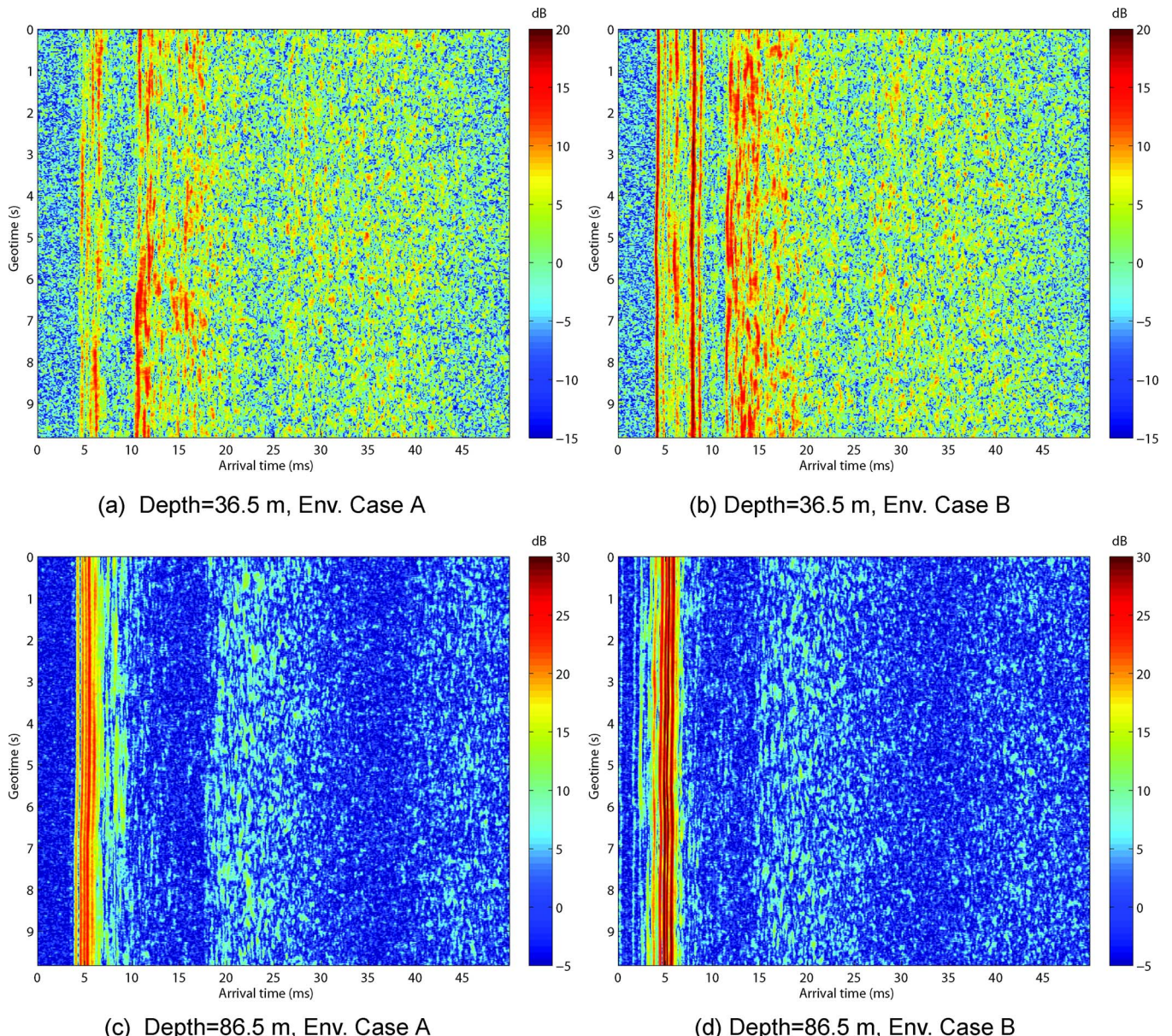


FIG. 6. (Color online) Estimated CIR functions at 36.5 m below the sea surface are shown (a) at 12:00 and (b) at 23:00 on July 2, 2003. Estimated CIR functions at 86.5 m below the sea surface are shown (c) at 12:00 and (d) at 23:00 on July 2, 2003. Note that the color scale of subplots (a) and (b) has a different dynamic range than that of subplots (c) and (d).

duration of a data packet. Note that time reversal combining alone with frequent channel updates previously has been discussed.²⁴ Joint time reversal combining and multichannel equalization also has been considered with emphasis on the use of low-complexity multichannel combining algorithms.²⁵

In the multichannel DFEs developed by Stojanovic *et al.*, feedforward filters are applied to the individual channels and their outputs are combined prior to the feedback filter.²³ Phase synchronization at the individual channels is optimized jointly with the equalizer tap weights. The number of adaptive feedforward taps increases with the number of channels. Compared with the multichannel DFEs developed by Stojanovic *et al.*, the proposed receiver uses a single channel DFE after time reversal combining.

An advantage of the proposed receiver structure is its low complexity.²⁶ The complexity of a multichannel DFE in-

creases at least as the square of the number of channels if RLS algorithms are used for a fast tracking capability.²² Since time reversal combining collapses multiple channels into a single channel, the complexity of the successive DFE remains unchanged when the number of channels increases. The complexity of the channel estimators increases linearly with the number of channels. It also increases linearly with the number of taps estimated for each channel if a fast least squares algorithm, such as the LSQR algorithm, is employed.

To measure the receiver performance, the SNR at the soft output $\tilde{x}(n)$, denoted by ρ_{out} , is used. In the next section, the output SNR of the receiver is shown for the 27 h period during KauaiEx.

TABLE I. Receiver parameters.

Parameters	Description	Value
f_s	Sampling rate	50 kHz
f_c	Carrier frequency	12 kHz
R	Symbol rate	4 kHz
f_{EB}	Excess bandwidth of the square-root raised cosine filter	4 kHz
K	Oversampling factor	3
M	Total number of the channels	4 or 10
N_{preamble}	Size of the preamble	1000 symbols
L	Length of the CIR function	200 symbols
N_0	Channel estimation block size	400 symbols
N	Channel estimation update interval	100 symbols
N_Δ	Doppler observation block size	400 symbols
δf_0	Initial Doppler search range	10 Hz
δf	Doppler search range after the preamble	1.6 Hz
N_{ff}	Feedforward filter span in symbols	15 symbols
N_{fb}	Feedback filter tap number	8 symbols
K_{f_1}	Proportional tracking constant in PLL	0.0002
K_{f_2}	Integral tracking constant in PLL	0.0002
λ	RLS forgetting factor in the DEF	0.999

IV. THE RECEIVER PERFORMANCE IN KAUAIEX

A. Acoustic channels on the MPL array

Due to the large aperture and deployment range of the MPL array, the CIR functions at the top and at the bottom of the array show different characteristics. For example, Fig. 5(b) shows the CIR function across the MPL array at 12:00 on July 2, 2003. The CIR function is obtained from the received LFM signals. Based on the ray diagram generated by the BELLHOP model²⁸ with the downward refracting sound speed profile in Fig. 5(a), it can be seen that the CIR function at the top hydrophone is composed of direct (D), bottom (B), surface (S), B-S, S-B, and S-B-S paths, etc. Most ray paths have surface interaction. In contrast, the CIR function on the bottom hydrophone consists primarily of multiple bottom interacting arrivals.

As a consequence of the different propagation paths, the

CIR functions in the upper water column have different energy levels and temporal coherence properties from those in the lower water column. Figure 6 shows a comparison of the CIR functions in the upper and lower water column for two data packets during two different environmental conditions. The CIR functions are obtained by the channel estimator in the receiver. Note that the color scale of subplots (a) and (b) represents a dynamic range from -15 to 20 dB, whereas that of subplots (c) and (d) represents a dynamic range from -5 to 30 dB. The energy of the CIR function in the lower water column is much higher than that in the upper water column. The input SNR is 12.4 dB at 36.5 m depth while it is 18.5 dB at 86.5 m depth. When environmental Case A changes to Case B, the CIR functions both in the upper and in the lower water column change. At 23:00 on July 2 during environmental Case B, the CIR functions in Figs. 6(b) and 6(d) show stronger ray paths that do not interact with the sea surface. The input SNR at 36.5 m depth increases to 16.0 dB and that at 86.5 m depth increases to 22.6 dB.

To compare the performance of the communications data simultaneously recorded in the upper and the lower water column, the top 10 hydrophones of the MPL array (MPL-TOP) and the bottom 4 hydrophones of the MPL array (MPL-BTM) are considered as sub-arrays in the analysis because the CIR functions at these two sets of hydrophones show a similar arrival structure among themselves.

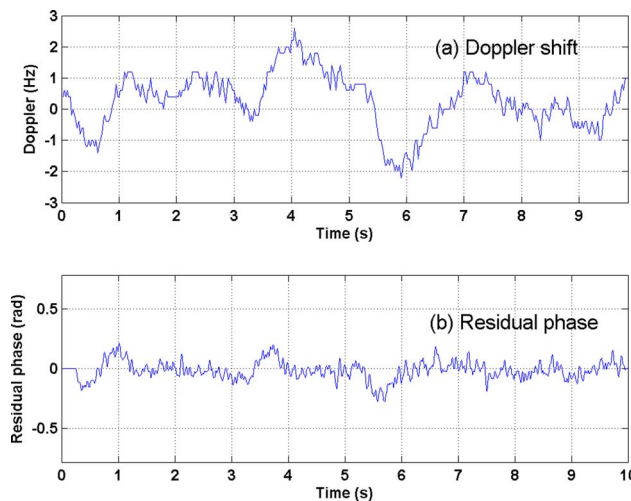


FIG. 7. (Color online) Doppler shift and phase fluctuations. (a) The Doppler estimate at 36.5 m below the sea surface and (b) the residual phase estimated by the PLL in the DFE on the MPL-TOP array at 23:00 on July 2, 2003.

B. The receiver performance

To compare the receiver performance on the MPL-TOP and MPL-BTM arrays in different environments, a uniform set of receiver parameters are chosen as in Table I. As mentioned, the element data are oversampled in the receiver and the oversampling rate is $K=3$. The number of the feedforward taps is KN_{ff} for the fractionally spaced DFE¹ where N_{ff} is the feedforward filter span in symbols. The number of the feedback taps is N_{fb} because the feedback filter is applied to a symbol spaced sequence, i.e., previously detected symbols.

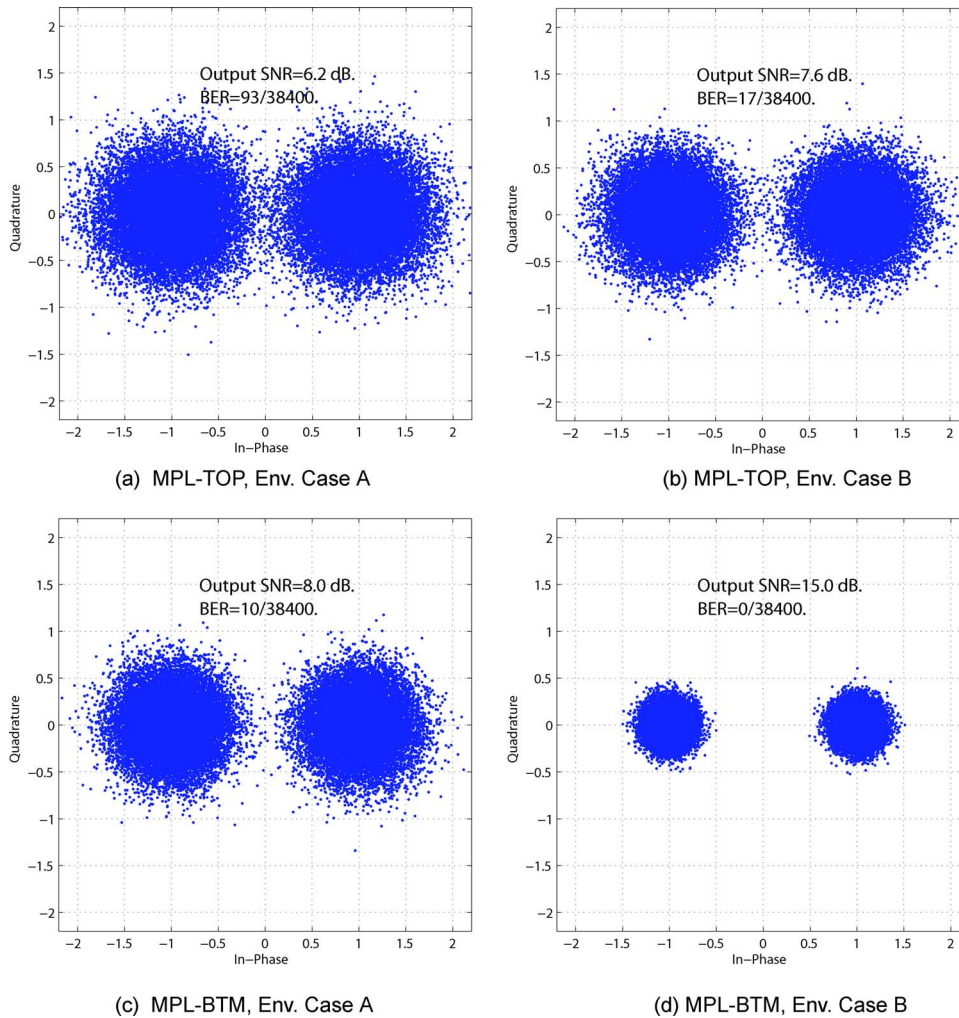


FIG. 8. (Color online) Scatter plots of the soft output $\tilde{x}(n)$ for the MPL-TOP array are shown (a) at 12:00 and (b) at 23:00 on July 2, 2003. Scatter plots of the soft output $\tilde{x}(n)$ for the MPL-BTM array are shown (c) at 12:00 and (d) at 23:00 on July 2, 2003.

The receiver parameters are optimized against fast channel fluctuations on the MPL-TOP array. For example, the channel estimation update interval is chosen as $N=100$ symbols, which is necessary for the MPL-TOP array receiver. In other words, channel and Doppler estimation is performed every 25 ms. As shown in Figs. 6(a) and 6(b), the CIR functions on the MPL-TOP array show significant fluctuations. Increasing N to 200 or 400 symbols deteriorates receiver performance for the MPL-TOP array while it does not affect receiver performance for the MPL-BTM array.

Frequent Doppler tracking and correction is also found necessary. As an example, Fig. 7(a) shows the observed time-varying Doppler shift (linear trend in the carrier phase offset) at a MPL-TOP array element during a single packet. Figure 7(b) shows the residual phase estimated by the PLL in the DFE when the Doppler tracking and correction is performed every 25 ms. Because of explicit Doppler tracking, the residual phase is small as shown. If the Doppler tracking and correction is only performed at the beginning of the packet, the receiver fails to track the channel and to demodulate the symbol sequence during 24 packets on the MPL-TOP array. If the Doppler tracking and correction is performed every 1 s, still there are 11 packets where the receiver fails to demodulate on the MPL-TOP array.

At the beginning of the 10 s BPSK packet, $N_{\text{preamble}} = 1000$ symbols are used to carry out initial channel estima-

tion, Doppler tracking, and DFE tap weight training. During the preamble, the initial Doppler search range is 10 Hz. As the Doppler shift is being tracked, the Doppler search range after the preamble is set relatively small, 1.6 Hz. The search step is 0.2 Hz. Therefore, the complexity introduced by Doppler tracking is very limited. The RLS forgetting factor λ in the DFE is chosen as 0.999.

Figure 8 shows the receiver performance for the MPL-TOP and MPL-BTM arrays during the two environmental cases. When the environment changed from Case A to Case B, the MPL-TOP array receiver performance improves slightly as shown in Figs. 8(a) and 8(b). The output SNR at 12:00 on July 2 during environmental Case A is 6.2 dB, whereas that at 23:00 on July 2 during environmental Case B is 8 dB. In contrast, the MPL-BTM array receiver performance improves significantly between environmental Case A and Case B with the output SNR increasing 7.0 dB.

Figure 9 shows the output SNR for the MPL-TOP and MPL-BTM arrays for the entire 27 h recording period. As shown in Fig. 2, the environmental characteristics changed significantly over this period as did receiver performance. For the MPL-BTM array, the average output SNR increases 5.8 dB from environmental Case A to environmental Case B. In contrast, for the MPL-TOP array, the average output SNR experiences a much smaller increase (1.8 dB) between these

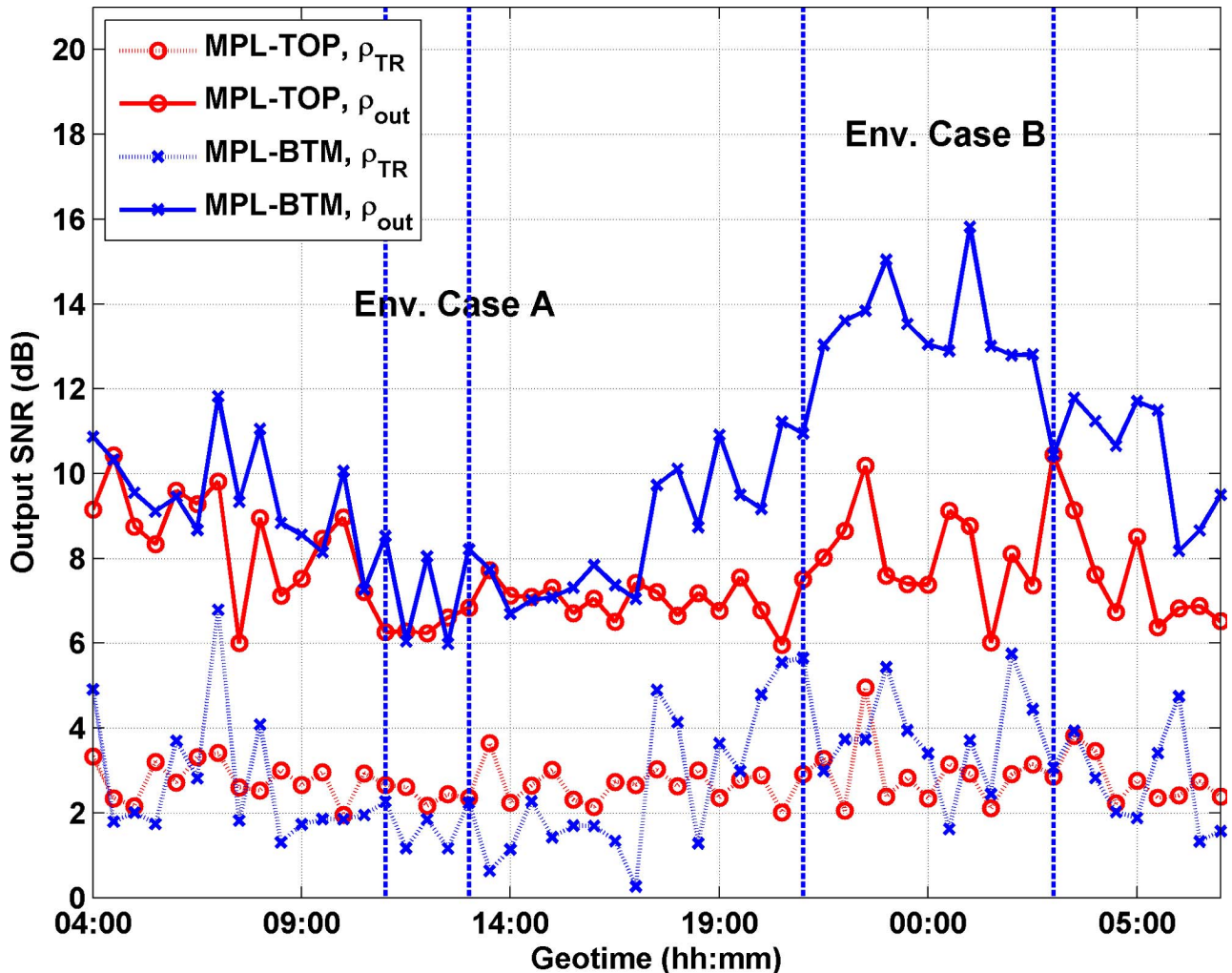


FIG. 9. (Color online) The output SNR for the MPL-TOP and MPL-BTM arrays from 04:00 on July 2 to 07:00 on July 3, 2003. For the MPL-BTM array, the average output SNR increases 5.8 dB during the change from environmental Case A to environmental Case B. In contrast, for the MPL-TOP array, the average output SNR experiences a much smaller increase (1.8 dB) when the environment changes from Case A to Case B. The intermediate SNR ρ_{TR} at the output of time reversal combining also is shown. Improvements using a DFE after time reversal combining are clearly.

cases. The primary distinction between these periods is the well-mixed water column during environmental Case A and the downward refracting sound speed profile during environmental Case B.

The output $r(n)$ after time reversal combining already provides an estimate of the transmitted symbols.²⁴ The SNR of $r(n)$ after phase correction²⁴ is defined as ρ_{TR} . Through a comparison between ρ_{TR} and ρ_{out} , the benefit of channel equalization after time reversal combining can be seen. As shown in Fig. 9, postprocessing $r(n)$ with a DFE on the MPL-TOP and MPL-BTM arrays can improve the performance for all BPSK packets. For the MPL-TOP array, the improvement is 4.9 dB for the entire MPL array recording period and the improvement is roughly uniform along geotime. In contrast, for the MPL-BTM array, the average improvement through use of a DFE is about 7.1 dB and the improvement varies during different environmental conditions. During environmental Case B, the improvement is as high as 9.3 dB.

It is worthwhile to note that although the water column and sea surface conditions vary during the 27 h period, the

channel can be tracked and the bit error rate is below 10^{-2} for all 55 packets. For 9 packets on the MPL-TOP array and 29 packets on the MPL-BTM array, there are no demodulation errors.

As shown in Fig. 9, even with ten hydrophones, the receiver with the MPL-TOP array usually has inferior performance to that with the MPL-BTM array, which only has four hydrophones. As the water column sound speed environment changes from well-mixed to downward refracting, the MPL-BTM array is more strongly insonified.²⁹ In addition, on the MPL-TOP array, most acoustic arrivals have sea surface interaction so that these arrivals are weaker and have shorter temporal coherence.

V. CONCLUSIONS

During KauaiEx, 27 h of high frequency acoustic communications measurements centered at 12 kHz and environmental observations were made in 100 m depth water near Kauai, Hawaii. The acoustic channels in KauaiEx exhibited challenging features including severe multi-path spread and

fast fluctuations. To overcome these difficulties, the BPSK data with a symbol rate of 4 kilosymbols/s were demodulated by time reversal multichannel combining followed by a single channel DFE. Continuous channel updates along with Doppler tracking on the individual channels were required prior to time reversal combining.

The proposed receiver was applied to the communications data obtained for two subsets of array elements whose channel characteristics appear distinct: (1) top 10 and (2) bottom 4 elements of a 16 element array spanning the entire water column. With the aide of the 1000 symbol preamble, all BPSK packets can be demodulated successfully using both sets of array elements. The resulting communications performance in terms of output SNR exhibited significant change over the 27 h transmission duration. This is particularly evident as the water column changed from well-mixed to a downward refracting environment.

ACKNOWLEDGMENTS

This research was supported by the Office of Naval Research (ONR) Code 321OA. The KauaiEx Group consists of Michael B. Porter, Paul Hursky, Martin Siderius (Heat, Light, & Sound Research Inc.), Mohsen Badiey (University of Delaware), Jerald Caruthers (University of Southern Mississippi), William S. Hodgkiss, Kaustubha Raghukumar (Scripps Institution of Oceanography), Daniel Rouseff, Warren Fox (University of Washington), Christian de Moustier, Brian Calder, Barbara J. Kraft (University of New Hampshire), Vincent McDonald (SPAWAR), Peter Stein, James K. Lewis, and Subramaniam Rajan (Scientific Solutions Inc.).

- ¹M. Stojanovic, J. A. Catipovic, and J. G. Proakis, "Phase-coherent digital communications for underwater acoustic channels," *IEEE J. Ocean. Eng.* **19**, 100–111 (1994).
- ²M. Stojanovic, J. Catipovic, and J. G. Proakis, "Adaptive multichannel combining and equalization for underwater acoustic communications," *J. Acoust. Soc. Am.* **94**, 1621–1631 (1993).
- ³M. Stojanovic, L. Freitag, and M. Johnson, "Channel-estimation-based adaptive equalization of underwater acoustic signals," *Oceans* (IEEE, New York, 1999), Vol. 2, pp. 590–595.
- ⁴A. Parvulescu and C. S. Clay, "Reproducibility of signal transmissions in the ocean," *Radio Electron. Eng.* **29**, 223–228 (1965).
- ⁵A. Parvulescu, "Matched-signal ("MESS") processing by the ocean," *J. Acoust. Soc. Am.* **98**, 943–960 (1995).
- ⁶W. A. Kuperman, W. S. Hodgkiss, H. C. Song, P. Gerstoft, P. Roux, T. Akal, C. Ferla, and D. R. Jackson, "Ocean acoustic time reversal mirror," *Proceedings of the Fourth European Conference Underwater Acoustics*, 1998, pp. 493–498.
- ⁷G. F. Edelmann, T. Akal, W. S. Hodgkiss, S. Kim, W. A. Kuperman, and H. C. Song, "An initial demonstration of underwater acoustic communications using time reversal," *IEEE J. Ocean. Eng.* **31**, 602–609 (2002).
- ⁸H. C. Song, P. Roux, W. S. Hodgkiss, W. A. Kuperman, T. Akal, and M. Stevenson, "Multiple-input/multiple-output coherent time reversal communications in a shallow water acoustic channel," *IEEE J. Ocean. Eng.* **31**, 170–178 (2006).

- ⁹D. Rouseff, D. R. Jackson, W. L. J. Fox, C. D. Jones, J. A. Ritcey, and D. R. Dowling, "Underwater acoustic communication by passive-phase conjugation: Theory and experimental results," *IEEE J. Ocean. Eng.* **26**, 821–831 (2001).
- ¹⁰T. C. Yang, "Temporal resolutions of time-reversal and passive-phase conjugation for underwater acoustic communications," *IEEE J. Ocean. Eng.* **28**, 229–245 (2003).
- ¹¹T. C. Yang, "Differences between passive-phase conjugation and decision-feedback equalizer for underwater acoustic communications," *IEEE J. Ocean. Eng.* **29**, 472–487 (2004).
- ¹²G. F. Edelmann, H. C. Song, S. Kim, W. S. Hodgkiss, W. A. Kuperman, and T. Akal, "Underwater acoustic communications using time reversal," *IEEE J. Ocean. Eng.* **30**, 852–864 (2005).
- ¹³T. C. Yang, "Correlation-based decision-feedback equalizer for underwater acoustic communications," *IEEE J. Ocean. Eng.* **30**, 865–880 (2005).
- ¹⁴H. C. Song, W. S. Hodgkiss, W. A. Kuperman, M. Stevenson, and T. Akal, "Improvement of time reversal communications using adaptive channel equalizers," *IEEE J. Ocean. Eng.* **31**, 487–496 (2006).
- ¹⁵H. C. Song, W. S. Hodgkiss, W. A. Kuperman, W. J. Higley, K. Raghukumar, and T. Akal, "Spatial diversity in passive time reversal communications," *J. Acoust. Soc. Am.* **120**, 2067–2076 (2006).
- ¹⁶N. M. Carbone and W. S. Hodgkiss, "Effects of tidally driven temperature fluctuations on shallow-water acoustic communications at 18 kHz," *IEEE J. Ocean. Eng.* **25**, 84–94 (2000).
- ¹⁷M. Badiey, Y. Mu, J. A. Simmen, and S. E. Forsythe, "Signal variability in shallow-water sound channels," *IEEE J. Ocean. Eng.* **25**, 492–500 (2000).
- ¹⁸T. C. Yang, "Measurements of temporal coherence of sound transmissions through shallow water," *J. Acoust. Soc. Am.* **120**, 2595–2614 (2006).
- ¹⁹M. B. Porter, P. Hursky, M. Siderius, M. Badiey, J. Caruthers, W. S. Hodgkiss, K. Raghukumar, D. Rouseff, W. Fox, C. de Moustier, B. Calder, B. J. Kraft, K. McDonald, P. Stein, J. K. Lewis, and S. Rajan, "The Kauai experiment," *High Frequency Ocean Acoustics* (AIP, New York, 2004), pp. 307–321.
- ²⁰M. Siderius, M. B. Porter, P. Hursky, V. McDonald, and the KauaiEx Group, "Effects of ocean thermocline variability on noncoherent underwater acoustic communications," *J. Acoust. Soc. Am.* **121**, 1895–1908 (2007).
- ²¹V. K. McDonald, P. Hursky, and the KauaiEx Group, "Telesonar testbed instrument provides a flexible platform for acoustic propagation and communication research in the 8–50 kHz band," *High Frequency Ocean Acoustics* (AIP, New York, 2004), pp. 336–349.
- ²²J. G. Proakis, *Digital Communications*, 4th ed. (McGraw-Hill, New York, 2000).
- ²³J. C. Preisig, "Performance analysis of adaptive equalization for coherent acoustic communications in the time-varying ocean environment," *J. Acoust. Soc. Am.* **118**, 263–278 (2005).
- ²⁴J. A. Flynn, J. A. Ritcey, D. Rouseff, and W. L. J. Fox, "Multichannel equalization by decision-directed passive phase conjugation: Experimental results," *IEEE J. Ocean. Eng.* **29**, 824–836 (2004).
- ²⁵M. Johnson, L. Freitag, and M. Stojanovic, "Improved Doppler tracking and correction for underwater acoustic communications," *ICASSP'97* (IEEE, New York, 1997), Vol. 1, pp. 575–578.
- ²⁶C. C. Paige, "Fast numerically stable computations for generalized linear least squares problems," SIAM (Soc. Ind. Appl. Math.) *J. Numer. Anal.* **16**, 165–171 (1979).
- ²⁷J. Gomes, A. Silva, and S. Jesus, "Joint passive time reversal and multichannel equalization for underwater communications," *OCEANS'06* (IEEE, New York, 2006).
- ²⁸M. B. Porter and Y. C. Liu, "Finite-element ray tracing," *Proceedings of the International Conference on Theoretical Computational Acoustics*, 1995, Vol. 2, pp. 947–956.
- ²⁹F. B. Jensen, W. A. Kuperman, M. B. Porter, and H. Schmidt, *Computational Ocean Acoustics* (Springer, New York, 2000).